molecules

MDPI

Article

An Unexpected Iron (II)-Based Homogeneous Catalytic System for Highly Efficient CO_2-to-CO Conversion under Visible-Light Irradiation

Zi-Cheng Fu [1,†], Cheng Mi [1,†], Yan Sun [1], Zhi Yang [1], Quan-Qing Xu [1] and Wen-Fu Fu [1,2,*]

1 College of Chemistry and Engineering, Yunnan Normal University, Kunming 650092, China; zichengfu101@sina.cn (Z.-C.F.); micheng121@sina.com (C.M.); sunyan19931110@163.com (Y.S.); kmyangz@sina.com (Z.Y.); qqxu1977@163.com (Q.-Q.X.)

2 Key Laboratory of Photochemical Conversion and Optoelectronic Materials and HKU-CAS Joint Laboratory on New Materials, Technical Institute of Physics and Chemistry, Chinese Academy of Sciences, Beijing 100190, China

* Correspondence: fuwf@mail.ipc.ac.cn

† These authors contributed equally to this work.

Received: 16 April 2019; Accepted: 13 May 2019; Published: 16 May 2019

Abstract: We present two as-synthesized Fe(II)-based molecular catalysts with 1,10-phenanthroline (phen) ligands; $Fe(phen)_3Cl_2$ (**1**) and $[Fe(phen)_2(CH_3CH_2OH)Cl]Cl$ (**2**), and their robust catalytic properties for the conversion of CO_2 to CO in DMF/TEOA (DMF = *N*,*N*′-dimethylformamide; TEOA = triethanolamine) solution containing $Ru(bpy)_3^{2+}$ and BIH (1,3-dimethyl-2-phenyl-2,3-dihydro-1*H*-benzo-[d]-imidazole). High turnover numbers (TONs) of 19,376 were achieved with turnover frequencies (TOFs) of 3.07 s^{-1} for complex **1** (1.5×10^{-7} M). A quantum efficiency of 0.38% was observed after 5 h irradiated by 450 nm monochromatic light. The generation rate of CO_2 and H_2 were tuned by optimizing the experimental conditions, resulting in a high CO selectivity of 90%. The remarkable contribution of the photosensitizer to the total TON_{CO} was found being 19.2% (as shown by tests under similar conditions without catalysts) when BIH was employed as a sacrificial electron donor. The product selectivity in complex **2** reached 95%, and the corresponding TON_{CO} and TOF_{CO} were 33,167 and 4.61 s^{-1} in the same concentration with complex **1** used as catalyst; respectively. This work provides guidance for future designs of simple, highly efficient and selective molecular catalytic systems that facilitate carbon-neutral solar-to-fuel conversion processes

Keywords: Fe-based catalyst; Ru(II) complex; photocatalysis; CO_2 reduction; CO

1. Introduction

Solar-light-driven reduction of CO_2 into energy-rich carbon-based products has attracted wide attention, with specific importance attached to the development of highly efficient catalysts and the establishing new photocataytic systems [1,2]. However, activation and conversion of CO_2 into desirable fuel or feedstock chemicals driven by visible light remains a significant challenge [3–7]. One way to promote the transformations is to employ heterogeneous [8–10] or homogeneous catalyst [11–13]. In 1986, Lehn and co-workers reported the photocatalytic reduction of CO_2 with Co polypyridine complex as the catalyst in a homogeneous system [14]. Whereafter, a series of Ru(II)-Re(I) binuclear complexes linked by bridging ligands were then studied by Ishitani's group, and the TON of photocatalytic reduction of CO_2 to CO was increased from previously reported 170 to 232 [15,16]. Nevertheless, it is economic and popular to utilize the noble-metal-free complexes as catalysts rather than noble metal. In the regard, homogeneous catalytic systems with excellent potential in

visible-light-driven reduction of CO_2 to CO [17–19] were developed using Fe [9,20–22], Co [23–25], Ni [26–28], Cu [29–31] and Mn [32–34] complexes as catalysts.

A stunning homogeneous molecular system containing nickel *N*-heterocyclic carbene-isoquinoline complex employed as catalyst, iridium complex as photosensitizer (PS) towards photocatalytic transformation of CO_2 to CO was successfully established [35]. This system exhibited a high photocatalytic performance of CO_2 to CO with TONs up to 98,000 and a TOF reaching 3.9 s^{-1} for a very low concentration of the catalyst, implying high catalytic sensitivity to the CO_2 reduction reaction. Recently, Lau and co-workers reported another highly efficient and selective system that consists of $Ru(bpy)_3^{2+}$, Fe(II) or Co(II) quaterpyridine complex in the presence of two electron donors; BIH, the higher TON_{CO} than 3000 with up to 95% selectivity was observed for the iron catalyst [36]. Due to rare characteristics of Ru and Ir, the homogeneous system involving earth-abundant metal complexes for photocatalytic reduction of CO_2 was then constructed by Ishitani's group using Cu(I) $Cu(dmp)(P)_2^+$ (dmp = 2,9-dimethyl-1,10-phenanthroline; P = phosphine ligand) as the PS and $[Fe(dmp)_2(NCS)_2]^{2+}$ as the catalyst [37]. The TON_{CO} of 273 and quantum yield of 6.7% were observed with selectivity of the CO up to 70.5%. Among molecular catalysts for the CO_2-to-CO conversion, a macrocyclic amine cryptate dinuclear cobalt complex has been shown to be robust, using $Ru(phen)_3^{2+}$ as the PS, the TON reached 16,896 with a quantum efficiency of 0.04% [38].

Herein, we report a highly efficient and selective homogeneous visible-light-driven catalytic system for CO_2-to-CO conversion. This includes as-synthesized Fe-based complexes employed as the catalysts, Ru(II) complex as the PS and BIH as the electron donor in DMF/TEOA (Scheme 1). An investigation into catalytic efficiency and selectivity between CO and H_2 was performed for various concentrations of catalyst, PS and BIH, and different ratios of DMF/TEOA. The corresponding mechanism was also suggested.

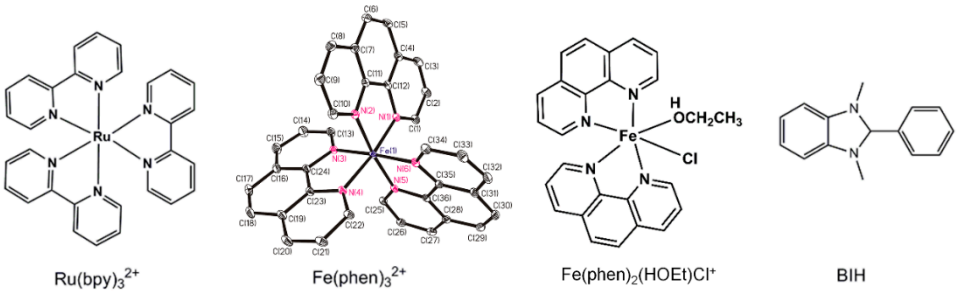

Scheme 1. Structures of the photosensitizer, catalysts, and BIH.

2. Results and Discussion

2.1. Characterization of Catalysts and Electrochemical Property

$Fe(phen)_3Cl_2$ (**1**), $[Fe(phen)_2(CH_3CH_2OH)Cl]Cl$ (**2**) and BIH [39] were prepared according to a modification of published procedures. All of these compounds were characterized by MS, ^1H NMR spectroscopy and elemental analysis (see the section of materials and methods, Figure S1 in the Supplementary Materials). The crystal structure of $Fe(phen)_3Cl_2$ was determined by single-crystal X-ray diffraction analysis (Figure S2 and Table S1). The cyclic voltagrammetry of $Fe(phen)_3Cl_2$ was recorded in a DMF solution containing 0.1 M $^nBu_4NPF_6$ under an Ar atmosphere at ambient temperature (Figure S3). Figure S3 shows three distinct redox waves at −1.05, −1.21 and −1.44 V vs. NHE, with these tentatively attributed to $Fe^{II}(phen)_3/Fe^{I}(phen)_3$, $Fe^{I}(phen)_3/Fe^{0}(phen)_3$ and $Fe^{0}(phen)_3/Fe^{0}(phen)_2(phen^{\cdot-})$, respectively [40]. After CO_2 bubbling to the system, two irreversible reduction waves underwent slight negatively shifts from −1.05 and −1.21 V to −1.08 and −1.32 V, respectively. There was a remarkable current enhancement for the latter, consistent with the electrocatalytic CO_2 reduction (Figure S3) [41,42].

2.2. Catalyst-Concentration Dependence of Phtocatalytic CO_2-to-CO Conversion for $Fe(phen)_3Cl_2$ (1)

The photocatalytic reduction systems were assembled using $Ru(bpy)_3^{2+}$, complex **1** and BIH in a CO_2-saturated DMF/TEOA solution. The produced gas products were identified using gas chromatography (GC), with Ar as carrier gas. The generating rates of CO and H_2 were determined as a function of catalyst concentration. The results in Figure 1 clearly show that the production of CO and H_2 was enhanced with increasing catalyst concentrations, and reaction system was accompanied by a H_2-generating reaction that becomes less important at higher catalyst concentrations. In comparison to results for a lower catalyst concentration (3.0×10^{-8} M) where 4.25 μmol CO was produced with a selectivity of 68% after 2 h of visible-light irradiation, and a higher catalyst concentration of 3.0×10^{-5} M evolved 61.21 μmol CO at a selectivity of 92% (Table 1). Furthermore, 96.23 μmol of CO and a selectivity of 94% were achieved when the concentration of $Fe(phen)_3Cl_2$ reached 1.5×10^{-4} M, which clearly show that concentration of catalyst plays significant role to selectivity of CO_2-to-CO conversion. However, in the absence of the Fe(II) complex, small amounts of CO and H_2 were detected, with the H_2-generation rate being superior to that of CO_2 reduction [43–45], indicating a significant contribution by the PS to the CO-generating rate and the effect on product selectivity (Table 1, entry 4) [46].

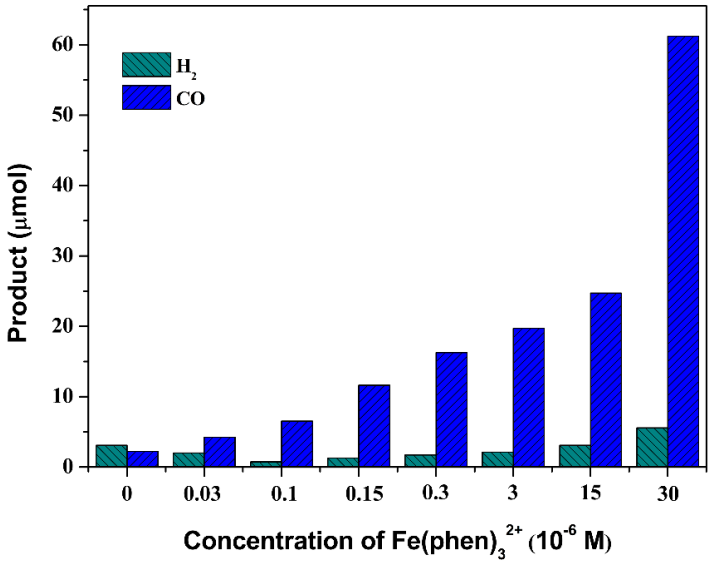

Figure 1. Catalyst-concentration dependence of CO and H_2 production in 4 mL CO_2-saturated DMF/TEOA solution (*v*/*v*, 7:1) containing 6.7×10^{-4} M $Ru(bpy)_3^{2+}$ and 0.022 M BIH after bright LED visible-light irradiation for 2 h at 298 K.

Table 1. Controlled experimental results from $Fe(phen)_3Cl_2$ (**1**) for photocatalytic conversion of CO_2 to CO.

Entry	[cat. 1] μM	[ps] mM	CO μmol	H_2 μmol	Selectivity of CO	TON_{CO}
1	0.03	0.67	4.25	2.00	68.0%	35,417
2	0.15	0.67	11.62	1.29	90.0%	19,367
3	0.15	0.00	0.00	0.06	0	0
4	0.00	0.67	2.23	3.09	41.9%	[a] 0.83
[b] 5	0.15	0.67	0.00	1.50	0	0
[c] 6	0.15	0.67	0.00	0.07	0	0
[d] 7	0.15	0.67	0.00	0.00	0	0
8	3.00	0.67	19.70	2.11	90.3%	1642
9	30	0.67	61.21	5.57	91.7%	510
10	150	0.67	96.23	5.88	94.2%	160

[a] TON value only determined from the PS; [b] Without CO_2; [c] Under dark conditions; [d] Without TEOA. Reaction conditions: LED light irradiation for 2 h, 4 mL CO_2-saturated DMF/TEOA solution (*v*/*v*, 7:1), 0.022 M BIH.

2.3. The Dependence of the Photocatalytic Reduction Rates on PS for Catalyst (1)

To evaluate the catalytic capacity of the catalysts towards CO_2 reduction and accompanied H_2 production, the dependence of the photocatalytic reduction rates on PS concentration was conducted at a fixed concentration of $Fe(phen)_3Cl_2$ and various irradiation time. Figure S4 demonstrates that higher conversion efficiencies of CO_2-to-CO were achieved after 6 h irradiation of the reaction system containing $Fe(phen)_3Cl_2$ (1.5×10^{-7} M) and BIH (0.022 M) with various PS concentrations. Increasing the amount of PS from 1.7×10^{-4} to 6.7×10^{-4} M significantly enhanced CO_2 conversion and H_2 evolution (Figure S5), with produced amounts of CO and H_2 increasing from 1.64 and 1.74 μmol to 16.63 and 3.45 μmol, respectively (Figures S4 and S5). However, the CO selectivity of 83% (irradiation time for 6 h), when compared with that for a solution at the same concentration of PS and catalyst (Table 1, entry 2), clearly showed that the main-product selectivity decreased for longer irradiation times, suggesting a change of catalytic active species during photochemical reaction. This probably results from the contribution of generated $Ru^{I}(bpy)_3{}^{+}$ species during photocatalytic reaction to CO_2-to-CO conversion and H_2 evolution.

2.4. Optimization of Reaction Conditions for Photocatalysis

Furthermore, optimized conditions for product selectivity were considered in a CO_2-saturated DMF/TEOA solution (*v/v*, 2.5:1) containing fixed amounts of PS and $Fe(phen)_3Cl_2$ at various BIH concentrations. As shown in Figure S6, the amount and selectivity of CO production strongly depends on the concentration of BIH and enhanced with increasing BIH concentration, reaching a limiting value at a scope of 0.022 M of BIH. Subsequent addition of BIH led to a negative relationship of photocatalytic efficiency, and H_2 even become dominant. Previous studies revealed that metal nanoparticles such as Fe [47] and Ni [48] may possibly be involved in the homogenous photocatalytic reduction reaction. Thus, considering that BIH has a stronger reducing ability ($E^{ox}{}_{1/2}$ = 0.33 V vs. SCE), the possibility of in situ formation of Fe or Ru nanoparticles was assessed by a dynamic light scattering experiment [39,49]. The analysis confirmed that nanosized particles were not found during the photocatalytic reaction (Figure S7). The influence of BIH concentration on the photocatalytic efficiency and product selectivity possibly originates from its intense reduction and proton transfer ability, changing the relative proportion of some active components in the system during the photochemical reaction. Additionally, we tentatively contributed the changes to involving effective one-electron transfer from BIH to the excited state of PS and subsequent electron transfer from $BI^{\bullet}$ to the related species such as Ru(II)*, Ru(I) or Fe(II) catalyst with proton loss from $BIH^{\bullet+}$ (see mechanistic interpretation). Compared with catalytic activity of Fe-based complex for CO_2-to-CO conversion, the accumulation of generated Ru(I) species as catalyst in the case of high concentration of BIH is disadvantageous for reduction efficiency of CO_2 in the investigated system [49]; a detailed study is still in progress. Further controlled experiments showed that no CO and H_2 were generated when any of the following components were absent: light, CO_2 or TEOA (Table 1).

As discussed above (Figure S6), the optimized concentration of BIH was 0.022 M. A typical example of the products as a function of irradiation time for a CO_2-saturated solution with and without catalyst was given in Figure 2. Upon bright white LED irradiation, little CO and H_2 were produced in the initial 15 min. We assumed that during this period, the phen ligand attached to the central Fe underwent photoinduced partial dissociation and/or a TEOA-substitution reaction to generate active-site-bearing catalytic species [50]. Figure 2 clearly demonstrates changes in the relative amounts of products for the competing pathways with time. Following the initial period, a higher CO-generating rate was observed. A TON of 19,367 was achieved under subsequent 105 min of light irradiation, with a TOF of 3.07 s^{-1} and a CO selectivity that reached 90% (Table 1, entry 2). Under the same conditions, the quantum yield of the photocatalytic reduction of CO_2 to CO was measured as 0.38% after 5 h of irradiation with 450 nm monochromatic light (Xe lamp, 15 A). The inset in Figure 2 demonstrates that although the contribution of PS to the total catalytic efficiency was less important (2.23 μmol of CO, 3.09 μmol of H_2), in the parallel catalytic reduction processes without $Fe(phen)_3Cl_2$ the Ru(II) complex

exhibited a relatively high catalytic activity for H_2 generation. The amount of H_2 generated for the catalytic system compared with those in the system containing catalyst suggested that $Fe(phen)_3Cl_2$ exhibited higher selectivity to CO than to H_2. Besides, the dependence of the calculated TON_{CO} on the catalyst concentration was not linear because of the sluggish kinetics involving multiple electrons and protons. High TONs of up to 35,417 after 2 h of irradiation were observed for $Fe(phen)_3Cl_2$ concentration as low as 3.0×10^{-8} M, which is consistent with previous results [35,36,51].

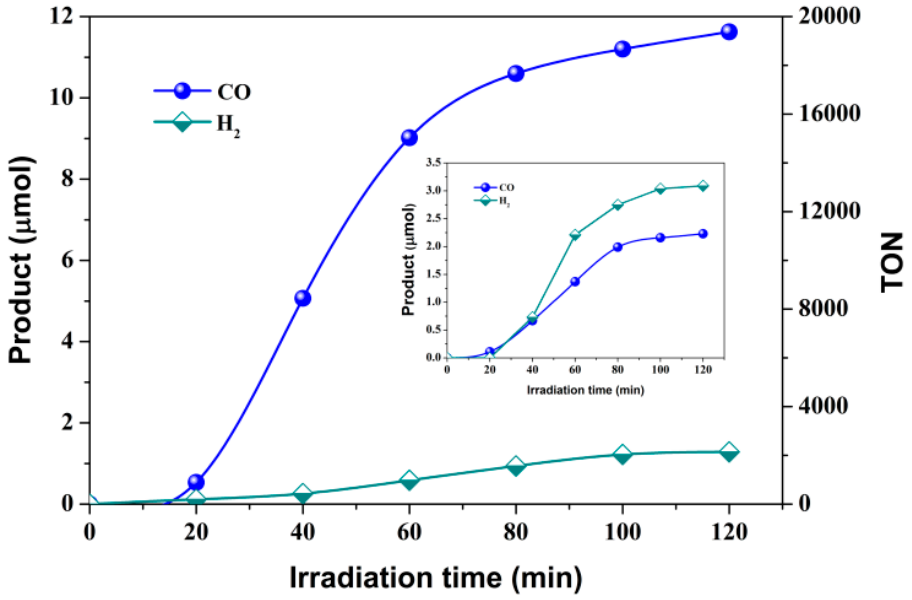

Figure 2. Evolution of CO (blue) and H_2 (dark cyan), and TON_{CO} during bright LED visible-light irradiation in 4 mL CO_2-saturated DMF/TEOA solution (*v*/*v*, 7:1) containing 6.7×10^{-4} M $Ru(bpy)_3^{2+}$, 0.022 M BIH and 1.5×10^{-7} M $Fe(phen)_3^{2+}$. Inset: without $Fe(phen)_3^{2+}$.

2.5. Comparison of Catalytic Efficiencies of CO_2-to-CO Conversion for Catalysts 1 and 2 and Isotopic Labeling Experiment

The catalytic activity of $[Fe(phen)_2(CH_3CH_2OH)Cl]Cl$ (**2**) was then evaluated under the same conditions. A comparison of the CO-evolution over 2 h of irradiation demonstrated that catalytic activity of complex **2** for the transformation of CO_2 to CO was greater than that of complex **1** (Figure 3). An unexpected high TON of 33,167 was achieved with a TOF of 4.61 s^{-1} for 1.5×10^{-7} M of catalyst **2**. When the catalyst concentration was increased to 3.0×10^{-5} M, 119.86 μmol of CO was generated, almost twice the number of times than that produced by catalyst **1** (61.21 μmol), with a CO selectivity of over 85% (Table S2). A comparison of TON_{CO} for catalytic performance of CO_2 reduction between catalyst **2** and Fe(II) quaterpyridine complex of previous report in different solvents [36], TON_{CO} values of 9,988 for the former (3.0×10^{-5} M, Table S2) and 1,879 for the latter (5.0×10^{-5} M) in the presence of $Ru(bpy)_3^{2+}$ and BIH, demonstrates that catalyst **2** used in the work exhibits higher catalytic activity for CO_2 reduction. Additionally, we found that the contribution of PS to CO_2-to-CO conversion is remarkable in the absence of Fe(II) complex catalyst when BIH is used as an electron donor, and the effect is enhanced with increasing concentration of BIH and the change of DMF/TEOA ratio (inset in Figure 2 and Figure S8). In order to identify the origin of the produced CO, an isotopic labeling experiment was conducted using $^{13}CO_2$ as the substrate on a GC-MS system under identical catalysis conditions [52,53]. As shown in Figure S9, the peak with m/z = 29 could be assigned to the reduced product of $^{13}CO_2$ and the m/z value of 45 was the original $^{13}CO_2$. These results confirmed that the CO evolution originated from the photocatalytic reduction of CO_2 and precluded possible degradation of organics used.

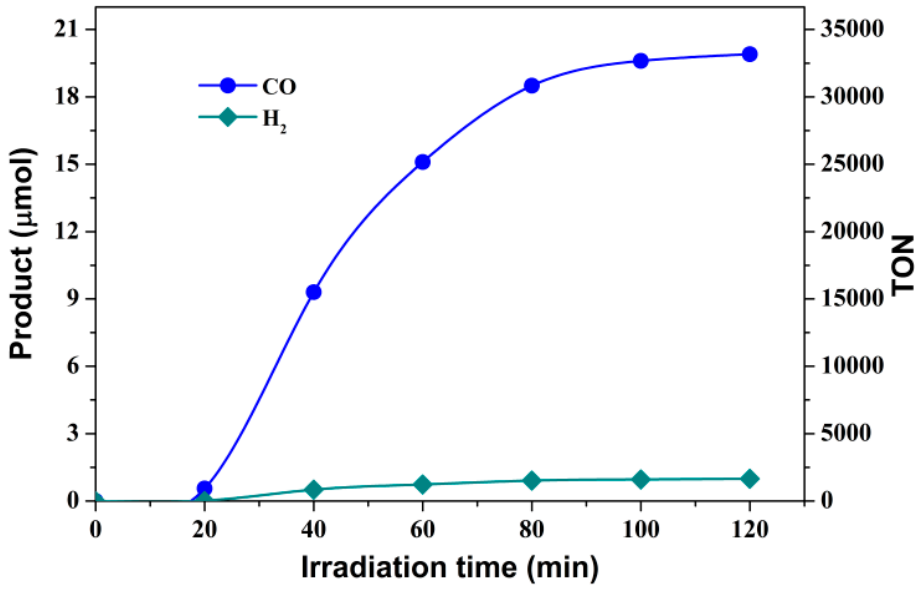

Figure 3. Visible-light-driven production of CO (blue) and H_2 (dark cyan) in 4 mL CO_2-saturated DMF/TEOA solution (*v*/*v*, 7:1) containing 6.7×10^{-4} M $Ru(bpy)_3^{2+}$, 0.022 M BIH and 1.5×10^{-7} M $Fe(phen)_2(CH_3CH_2OH)Cl^+$.

2.6. Detection of Reaction Intermediates and Mechanistic Interpretation

The detection and characterization of stable intermediates during the photoinduced reduction of CO_2 are of fundamental importance to the identification of the reaction mechanism leading to CO formation. High resolution mass spectrometry (HRMS) was therefore used to probe active intermediates under the given catalytic conditions. Figure 4 clearly shows a signal at *m*/*z* = 663.1272 in the positive mode, which was attributed to the intermediate $[Fe(phen)_3 + CO_2 + Na]^+$. Nevertheless, we did not observe a signal corresponding to $[Fe(phen)_2(TEOA) + CO_2 + Na]^+$ (*m*/*z* = 632.17). The HRMS results obtained can be considered as clear evidence for the interchange mechanism during CO_2 photoreduction. On the basis of these results, mechanism for photocatalytic CO_2-to-CO conversion by Fe-based complexes is proposed in Scheme 2. Upon excitation at visible light, the triplet excited state of PS was reductively quenched by BIH to give the one-electron reduced species, then the Fe(II) catalyst was doubly reduced to the active Fe(0) species. In such a case of lower oxidation state, we cannot distinguish whether the dissociation of ligand from the complex is anterior to formation of Fe-CO_2 adduct, but the intermediate $Fe(phen)_3 \cdots CO_2$ is observed by HRMS analysis. Thus, we speculate that this is accompanied by the contribution of one Fe-N bond breaking and Fe-CO_2 bond making in terms of an interchange of the ligand and CO_2, after which photodriven one-electron transfer from $Ru^I(bpy)_3^+$ to the adduct takes place, which needs to be protonated to cleave the C–OH bond, give CO, and regenerate $Fe^I(phen)_3^+$. It is noteworthy that in subsequent catalytic reactions, $BI^\bullet$ produced as an intermediate of sacrificial electron donor has strong reducing power (E^{ox} = −2.06 V vs. Fc^+/Fc), and donate performance. This is good agreement with experimental observation that in the initial stage there is remarkable induction period for H_2 and CO production. This means that the generated $BI^\bullet$ not only accelerates the formation of $Ru^I(bpy)_3^+$ but also probably directly transfers electron to Fe(II) catalyst to produce active catalytic species. Further studies on the contributions of PS to H_2 and CO evolution are in progress in our laboratory and will bring further insight into the solution of the problem.

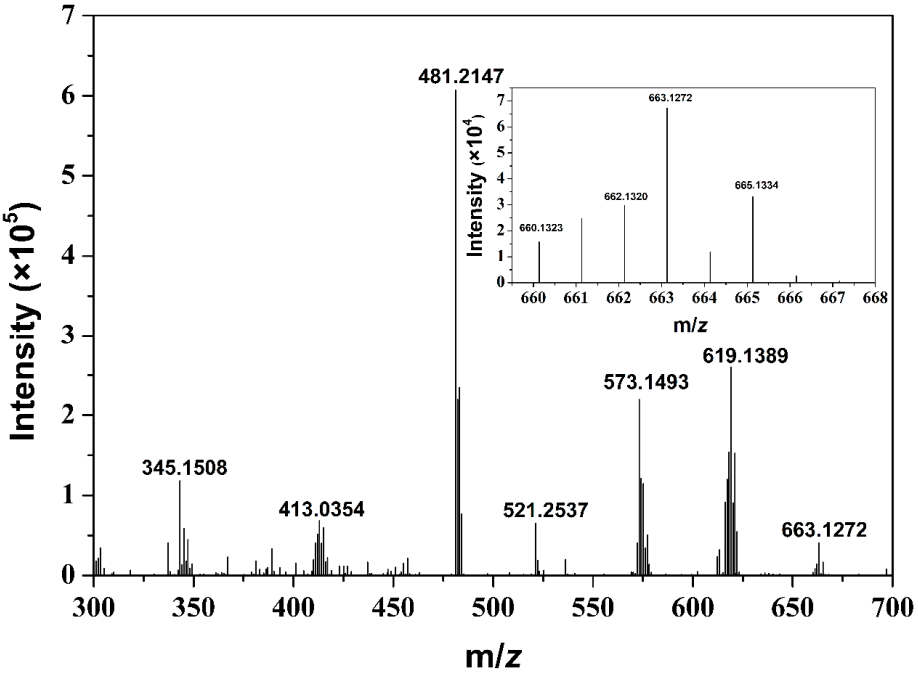

Figure 4. HRMS spectra of CO_2-saturated DMF/TEOA solution (*v*/*v*, 7:1) containing 0.67 mM $Ru(bpy)_3^{2+}$, 0.022 M BIH and 1.5×10^{-7} M $Fe(phen)_3^{2+}$ after irradiation for 30 min. Inset: measured isotopic distribution.

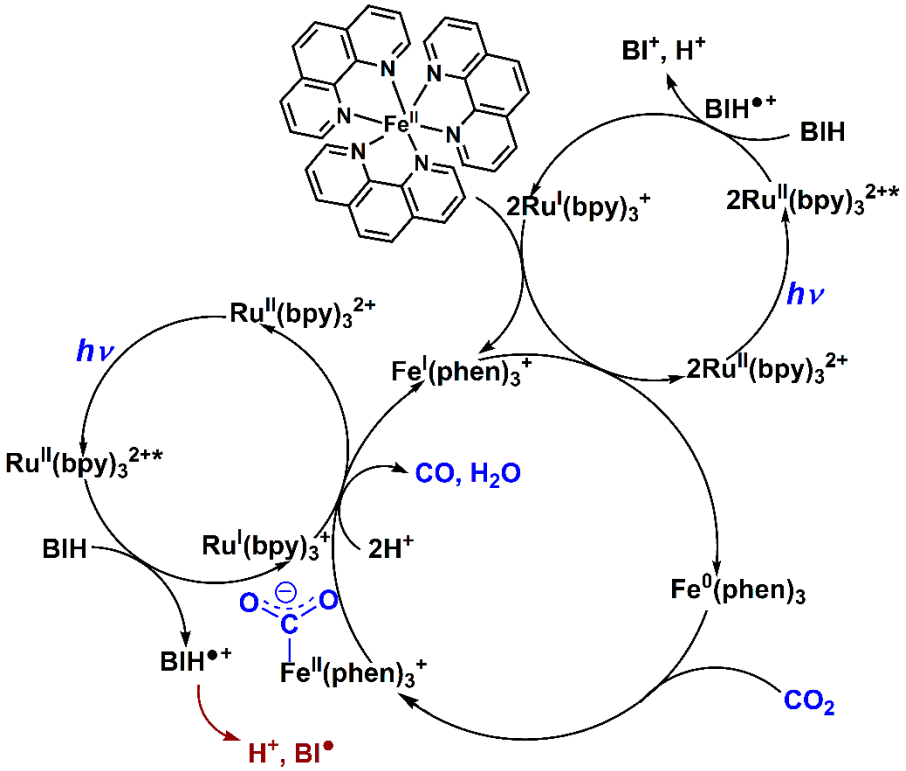

Scheme 2. Proposed mechanism of the photocatalytic CO_2-to-CO conversion for the presented system containing catalyst (**1**), $[Ru(bpy)_3]^{2+}$ and BIH.

3. Materials and Methods

3.1. Materials

Iron(II) chloride tetrhydrate (98%, Energy Chemical Ltd., Shanghai, China), 1,10-Phenanthroline (99%, J&K Scientific Ltd., Beijing, China), $[Ru(bpy)_3]Cl_2{\cdot}6H_2O$, 2-Phenylbenzimidazole (98%, J&K Scientific Ltd., Beijing, China), Iodomethane (97%, Ouhechem, Beijing, China), Sodium borohydride (99%, HuaDa, Guangdong, China). Sodium chloride, Sodium thiosulfate, Ethanol, Dichloromethane, Dithyl ether, *N*,*N*-Dimethylformamide, Triethanolamine come from Beijing Chemical Works (Beijing, China), and were used as purchased, without further purification.

3.2. Synthesis

The synthesis of $Fe(phen)_3Cl_2$ (**1**). Catalyst **1** was carried out as follows: $FeCl_2{\cdot}4H_2O$ (1.00 g, 5.03 mmol) and phen (2.72 g, 15.09 mmol) were added to 300 mL of ethanol and stirred under Ar overnight. The solvent was then removed by evaporation under vacuum. The solid product was purified by recrystallization at least four times in ethanol and ether. Yield: 90% (3.02 g). ^{1}H NMR (400 MHz, DMSO-d_6): δ = 8.81 (d, 6H, J = 8.0 Hz), 8.40 (s, 6H), 7.66–7.81 (m, 12H); ESI-MS (MeOH): m/z = 298.0692 $[M\text{-}2Cl]^{2+}$; elemental analysis calcd. for $C_{36}H_{24}N_6FeCl_2{\cdot}2H_2O$ (703.40): C 61.47, H 4.01, N 11.95; found: C 62.34, H 4.57, N 11.17.

$[Fe(phen)_2(CH_3CH_2OH)Cl]Cl$ (2). Catalyst **2** was synthesized and purified by a procedure similar to that used for **1**, except that 1.81 g (10.06 mmol) of phen was used. Yield: 74% (1.99 g). ^{1}H NMR (400 MHz, DMSO-d_6): δ = 8.81 (d, 4H, J = 8.0 Hz), 8.41 (s, 4H), 7.74 (dt, 8H J = 12.3, 5.0 Hz), 4.35 (t, 1H, J = 5.1 Hz), 3.38–3.50 (m, 2H), 1.06 (t, 3H, J = 7.0 Hz); ESI-MS (MeOH): m/z = 451.0422 $[M\text{-}Cl\text{-}CH_3CH_2OH]^+$; elemental analysis calcd. for $C_{26}H_{22}N_4OFeCl_2$ (533.23): C 58.56, H 4.16, N 10.51; found: C 59.28, H 4.45, N 10.61.

Synthesis of 1,3-dimethyl-2-phenyl-2,3-dihydro-1*H*-benzo-[d]-imidazole (BIH). NaOH (0.85 g, 21.3 mmol), 2-phenylbenzimidazole (2.9 g, 14.9 mmol) and CH_3I (7.9 g, 55.7 mmol) were dissolved in 20 mL of methanol with stirring for 20 min. The resulting solution was then transferred into a 50 mL Teflon-sealed autoclave and heated directly to 120 °C in an air-blowing thermostatic oven at a ramping rate of 5 °C min^{-1}; the temperature was maintained for 12 h. After cooling to room temperature, a white flake crystal (BI^+I^-) was obtained by filtration, and washing with deionized water and methanol. Thereafter, the solid sodium borohydride (567 mg, 15 mmol) was added slowly in batches to a solution containing 2.1 g of BI^+I^- (6 mmol) in methanol (80 mL) with stirring under an atmosphere of nitrogen at 273 K. After the reaction mixture was stirred for 2 h, reaction temperature was kept at 298 K, and processed for 1.5 h. Reaction solvent was then removed by distillation under reduced pressure, and 30 mL of deionized water was added. The resulting mixture was extracted with diethyl ether (3 × 30 mL), and the extractive was washed with the saturated aqueous solution of $Na_2S_2O_3$ and NaCl, respectively. The organic phase was dried over anhydrous $MgSO_4$ overnight. The filtration was concentrated to yield a white solid powder. ^{1}H NMR spectrum (400 MHz, $CDCl_3$): δ 7.84–7.35 (m, 5H), 6.82–6.33 (m, 4H), 4.93 (s, 1H), 2.61 (s, 6H). ESI-MS (MeOH): m/z = 223.1215 $(M + H)^+$.

3.3. Characterization

Single-crystal X-ray diffraction. Single crystals of $[Fe(phen)_3]Cl_2$ suitable for X-ray diffraction analysis were grown by slow evaporation of dichloromethane solutions, which allowed their molecular structures and packing modes in the solid state to be studied. CCDC reference number 1,571,123 contains the supplementary crystallographic data for this paper. These data can be obtained free of charge from The Cambridge Crystallographic Data Centre via www.ccdc.cam.ac.uk/data_request/cif.

Instrumentations. ^{1}H NMR spectra were recorded on a Bruker Avance 400 spectrometer with chemical shifts (δ, ppm) relative to tetramethylsilane. The mass spectra were determined on a Finnigan LCQ quadrupole ion trap mass spectrometer and a Shimadzu LCMS-IT-TOF mass spectrometer.

Elemental analyses were performed on a Vario EL III. The diffraction data of single crystal were collected on a Rigaku R-AXIS RAPID IP X-ray diffractometer using a graphite monochromator with Mo Kα radiation (λ = 0.071073 nm) at 113 K. Electrochemical measurements were carried out on a CHI660C electrochemical potentiostat. Dynamic light scattering measurement was carried out on a DynaPro NanoStar (Wyatt Technology Co., US).

3.4. Photocatalytic Experiments

The photocatalytic reduction of CO_2 to CO was conducted under 1 atm of CO_2 at 298 K. Typically, 4 mL of DMF/TEOA solution (*v/v*, 7:1) containing $[Ru(bpy)_3]Cl_2$, BIH, and Fe-based catalyst was added to a 18.5 mL cuvette sealed with a rubber septum placed on top of a magnetic stirrer. A stream of CO_2 was then passed into the reaction system for 30 min. White light-emitting diodes (LEDs) (30 × 3 W, $\lambda \geq 420$ nm) were used as the irradiation light source. The LEDs were positioned 3 cm away from the sample, which was kept under continuous stirring at room temperature. The generated gases were analyzed by a gas chromatography (GC-2014C, 5 Å molecular sieve column (3 m × 2 mm), DINJ 50 °C, DTCD 100 °C, column temperature 50 °C, carrier gas flow 30 mL/min). The amounts of products were determined using the external standard method as the basis for quantitative analysis. ^{13}C-labelled CO_2 experiments were performed following the same procedure and the gas products were analyzed by GC-TCD and GC-MS.

4. Conclusions

In summary, a highly efficient, visible-light-driven Fe-based catalytic system was established to reduce CO_2 to CO. Catalyst **2**, with its easily replaced ligands, displayed a catalytic activity twice as large as that of catalyst **1**, suggesting that the generated empty coordinating sites in the catalytic reduction of CO_2 play a crucial role. Generally, it is required that coordination-saturated Fe(II) complex catalysts proceed photoinduced reaction to generate active sites before forming Fe-CO_2 adduct, and the overall results are notable because the photodriven initial periods were similar for catalysts **1** and **2**. However, the results obtained from HRMS measurement indicate an interchange mechanism during CO_2 photoreduction for complex **1** as catalyst. The interrelationships among the components in the catalytic system, especially the effect of electron donor BIH on the contribution of PS to CO and H_2 generation, was therefore still further studied in detail. Undoubtedly, the higher selectivity and efficiency of the reported system for the visible-light-driven reduction of CO_2 to CO offers significant potential for carbon-neutral artificial photosynthesis cycles.

Supplementary Materials: Supplementary Materials are available online. Figures S1–S9, Tables S1–S2.

Author Contributions: Z.-C.F., C.M., and W.-F.F. designed research; Z.-C.F., C.M., Y.S., Z.Y., and Q.-Q.X. performed research and analyzed the data; and Z.-C.F., C.M., and W.-F.F. wrote the paper.

Funding: This work was financially supported by the Ministry of Science and Technology (2012DFH40090). We thank the National Natural Science Foundation of China (21777136, 21471155, 21367026) for financial support.

Conflicts of Interest: The authors declare no conflict of interest.

References

1. Morris, A.J.; Meyer, G.J.; Fujita, E. Molecular approaches to the photocatalytic reduction of carbon dioxide for solar fuels. *Acc. Chem. Res.* **2009**, *42*, 1983–1994. [CrossRef]
2. White, J.L.; Baruch, M.F.; Pander, J.E., III; Hu, Y.; Fortmeyer, I.C.; Park, J.E.; Zhang, T.; Liao, K.; Gu, J.; Yan, Y.; et al. Light-driven heterogeneous reduction of carbon dioxide: Photocatalysts and photoelectrodes. *Chem. Rev.* **2015**, *115*, 12888–12935. [CrossRef] [PubMed]
3. Dubois, M.R.; Dubois, D.L. Development of molecular electrocatalysts for CO_2 reduction and H_2 production/oxidation. *Acc. Chem. Res.* **2009**, *42*, 1972–1982.
4. Mahammadunnisa, S.; Reddy, P.M.K.; Ramaraju, B.; Subrahmanyam, C. Catalytic nonthermal plasma reactor for dry reforming of methane. *Energy Fuels* **2013**, *27*, 4441–4447.

5. Taheri, A.; Berben, L.A. Making C-H bonds with CO_2: Production of formate by molecular electrocatalysts. *Chem. Commun.* **2016**, *52*, 1768–1777. [CrossRef]
6. Asadi, M.; Kim, K.; Liu, C.; Addepalli, A.V.; Abbasi, P.; Yasaei, P.; Phillips, P.; Behranginia, A.; Cerrato, J.M.; Haasch, R.; et al. Nanostructured transition metal dichalcogenide electrocatalysts for CO_2 reduction in ionic liquid. *Science* **2016**, *353*, 467–470. [CrossRef]
7. Rao, H.; Bonin, J.; Robert, M. Toward visible-light photochemical CO_2-to-CH_4 conversion in aqueous solutions using sensitized molecular catalysis. *J. Phys. Chem. C* **2018**, *122*, 13834–13839. [CrossRef]
8. Indrakanti, V.P.; Kubickib, J.D.; Schobert, H.H. Photoinduced activation of CO_2 on Ti-based heterogeneous catalysts: Current state, chemical physics-based insights and outlook. *Energy Environ. Sci.* **2009**, *2*, 745–758. [CrossRef]
9. Xu, Y.F.; Yang, M.-Z.; Chen, B.-X.; Wang, X.-D.; Chen, H.-Y.; Kuang, D.-B.; Su, C.-Y. A $CsPbBr_3$ perovskite quantum dot/graphene oxide composite for photocatalytic CO_2 reduction. *J. Am. Chem. Soc.* **2017**, *139*, 5660–5663. [CrossRef]
10. Fu, Z.-C.; Xu, R.-C.; Moore, J.T.; Liang, F.; Nie, X.-C.; Mi, C.; Mo, J.; Xu, Y.; Xu, Q.-Q.; Yang, Z.; et al. Highly efficient photocatalytic system constructed from CoP/carbon nanotubes or graphene for visible-light-driven CO_2 reduction. *Chem. Eur. J.* **2018**, *24*, 4273–4278. [CrossRef]
11. Sen, P.; Mondal, B.; Saha, D.; Rana, A.; Dey, A. Role of 2nd sphere H-bonding residues in tuning the kinetics of CO_2 reduction to CO by iron porphyrin complexes. *Dalton. Trans.* **2019**, *48*, 5965–5977. [CrossRef]
12. Liu, X.; Inagaki, S.; Gong, L. Heterogeneous molecular systems for photocatalytic CO_2 reduction with water oxidation. *Angew. Chem. Int. Ed.* **2016**, *55*, 14924–14950. [CrossRef]
13. Sato, S.; Morikawa, T.; Kajino, T.; Ishitani, O. A highly efficient mononuclear iridium complex photocatalyst for CO_2 reduction under visible light. *Angew. Chem. Int. Ed.* **2013**, *52*, 988–992. [CrossRef]
14. Hawecker, J.; Lehn, J.M.; Ziessel, R. Photochemical and electrochemical reduction of carbon dioxide to carbon monoxide mediated by (2,2′-bipyridine)tricarbonylchlororhenium(I) and related complexes as homogeneous catalysts. *Helv. Chim. Acta.* **1986**, *69*, 1990–2012. [CrossRef]
15. Gholamkhass, B.; Mametsuka, H.; Koike, K.; Tanabe, T.; Furue, M.; Ishitani, O. Architecture of Supramolecular Metal Complexes for Photocatalytic CO_2 Reduction: Ruthenium−Rhenium Bi- and Tetranuclear Complexes. *Inorg. Chem.* **2005**, *44*, 2326–2336. [CrossRef]
16. Tamaki, Y.; Ishitani, O. Supramolecular photocatalysts for the reduction of CO_2. *ACS Catal.* **2017**, *7*, 3394–3409. [CrossRef]
17. Bonin, J.; Robert, M.; Routier, M. Selective and efficient photocatalytic CO_2 reduction to CO using visible light and an iron-based homogeneous catalyst. *J. Am. Chem. Soc.* **2014**, *136*, 16768–16771. [CrossRef]
18. Chen, L.J.; Guo, Z.G.; Wei, X.G.; Gallenkamp, C.; Bonin, J.; Mallart, E.A.; Lau, K.C.; Lau, T.C.; Robert, M. Molecular catalysis of the electrochemical and photochemical reduction of CO_2 with earth-abundant metal complexes. Selective production of CO vs. HCOOH by switching of the metal center. *J. Am. Chem. Soc.* **2015**, *137*, 10918–10927. [CrossRef]
19. Ouyang, T.; Hou, C.; Wang, J.W.; Liu, W.J.; Zhong, D.C.; Ke, Z.F.; Lu, T.B. A highly selective and robust Co(II)-based homogeneous catalyst for reduction of CO_2 to CO in CH_3CN/H_2O solution driven by visible light. *Inorg. Chem.* **2017**, *56*, 7307–7311. [CrossRef]
20. Bonin, J.; Chaussemier, M.; Robert, M.; Routier, M. Homogeneous photocatalytic reduction of CO_2 to CO using Iron(0) porphyrin catalysts: Mechanism and intrinsic limitations. *ChemCatChem* **2014**, *6*, 3200–3207. [CrossRef]
21. Hernández, A.R.; Steinlechner, C.; Junge, H.; Beller, M. Earth-abundant photocatalytic systems for the visible-light-driven reduction of CO_2 to CO. *Green Chem.* **2017**, *19*, 2356–2360.
22. Rao, H.; Schmidt, L.C.; Bonin, J.; Robert, M. Visible-light-driven methane formation from CO_2 with a molecular iron catalyst. *Nature* **2017**, *548*, 74–77. [CrossRef] [PubMed]
23. Dhanasekaran, T.; Grodkowski, J.; Neta, P.; Hambright, P.; Fujita, E. *p*-Terphenyl-sensitized photoreduction of CO_2 with cobalt and iron porphyrins. Interaction between CO and reduced metalloporphyrins. *J. Phys. Chem. A* **1999**, *103*, 7742–7748. [CrossRef]
24. Chan, S.L.F.; Lam, T.L.; Yang, C.; Yan, S.C.; Cheng, N.M. A robust and efficient cobalt molecular catalyst for CO_2 reduction. *Chem. Commun.* **2015**, *51*, 7799–7801. [CrossRef]
25. Chen, L.J.; Qin, Y.F.; Chen, G.; Li, M.Y.; Cai, L.R.; Qiu, Y.F.; Fan, H.B.; Robert, M.; Lau, T.C. A molecular noble metal-free system for efficient visible light-driven reduction of CO_2 to CO. *Dalton. Trans.* **2019**. [CrossRef]

26. Kuehnel, M.F.; Orchard, K.L.; Dalle, K.E.; Reisner, E. Selective photocatalytic CO_2 reduction in water through anchoring of a molecular Ni catalyst on CdS nanocrystals. *J. Am. Chem. Soc.* **2017**, *139*, 7217–7223. [CrossRef]
27. Hong, D.C.; Tsukakoshi, Y.; Kotani, H.; Ishizuka, T.; Kojima, T. Visible-light-driven photocatalytic CO_2 reduction by a Ni(II) complex bearing a bioinspired tetradentate ligand for selective CO production. *J. Am. Chem. Soc.* **2017**, *139*, 6538–6541. [CrossRef]
28. Lin, J.L.; Qin, B.; Fang, Z.X. Nickel bipyridine ($Ni(bpy)_3Cl_2$) complex used as molecular catalyst for photocatalytic CO_2 reduction. *Catal. Leet.* **2019**, *149*, 25–33. [CrossRef]
29. Angamuthu, R.; Byers, P.; Lutz, M.; Spek, A.L.; Bouwman, E. Electrocatalytic CO_2 conversion to oxalate by a copper complex. *Science* **2010**, *327*, 313–315. [CrossRef]
30. Guo, Z.G.; Yu, F.; Yang, Y.; Leung, C.-F.; Ng, S.M.; Ko, C.-C.; Cometto, C.; Lau, T.-C.; Robert, M. Photocatalytic Conversion of CO_2 to CO by a Copper(II) Quaterpyridine Complex. *ChemSusChem* **2017**, *10*, 4009–4013. [CrossRef]
31. Liu, W.-J.; Huang, H.-H.; Ouyang, T.; Jiang, L.; Zhong, D.-C.; Zhang, W.; Lu, T.-B. A Copper(II) Molecular Catalyst for Efficient and Selective Photochemical Reduction of CO_2 to CO in a Water-Containing System. *Chem. Eur. J.* **2018**, *24*, 4503–4508. [CrossRef]
32. Takeda, H.; Koizumi, H.; Okamoto, K.; Ishitani, O. Photocatalytic CO_2 reduction using a Mn complex as a catalyst. *Chem. Commun.* **2014**, *50*, 1491–1493. [CrossRef]
33. Torralba-Peñalver, E.; Luo, Y.; Compain, J.D.; Noblat, S.C.; Fabre, B. Selective catalytic electroreduction of CO_2 at silicon nanowires (SiNWs) photocathodes using non-noble metal-based manganese carbonyl bipyridyl molecular catalysts in solution and grafted onto SiNWs. *ACS. Catal.* **2015**, *5*, 6138–6147. [CrossRef]
34. Cheung, P.L.; Machan, C.W.; Malkhasian, A.Y.S.; Agarwal, J.; Kubiak, C.P. Photocatalytic reduction of carbon dioxide to CO and HCO_2H using fac-$Mn(CN)(bpy)(CO)_3$. *Inorg. Chem.* **2016**, *55*, 3192–3198. [CrossRef]
35. Thoi, V.S.; Kornienko, N.; Margarit, C.G.; Yang, P.D.; Chang, C.J. Visible-light photoredox catalysis: Selective reduction of carbon dioxide to carbon monoxide by a nickel N-heterocyclic carbene-isoquinoline complex. *J. Am. Chem. Soc.* **2013**, *135*, 14413–14424. [CrossRef]
36. Guo, Z.G.; Cheng, S.W.; Cometto, C.; Anxolabéhère-Mallart, E.; Ng, S.M.; Ko, C.C.; Liu, G.J.; Chen, L.J.; Robert, M.; Lau, T.C. Highly efficient and selective photocatalytic CO_2 reduction by iron and cobalt quaterpyridine complexes. *J. Am. Chem. Soc.* **2016**, *138*, 9413–9416. [CrossRef]
37. Takeda, H.; Ohashi, K.; Sekine, A.; Ishitani, O. Photocatalytic CO_2 reduction using Cu(I) photosensitizers with a Fe(II) catalyst. *J. Am. Chem. Soc.* **2016**, *138*, 4354–4357. [CrossRef]
38. Ouyang, T.; Huang, H.H.; Wang, J.W.; Zhong, D.C.; Lu, T.B. A dinuclear cobalt cryptate as a homogeneous photocatalyst for highly selective and efficient visible-light driven CO_2 reduction to CO in CH_3CN/H_2O Solution. *Angew. Chem. Int. Ed.* **2017**, *56*, 738–743. [CrossRef]
39. Zhu, X.Q.; Zhang, M.T.; Yu, A.; Wang, C.H.; Cheng, J.P. Hydride, hydrogen atom, proton, and electron transfer driving forces of various five-membered heterocyclic organic hydrides and their reaction intermediates in acetonitrile. *J. Am. Chem. Soc.* **2008**, *130*, 2501–2516. [CrossRef]
40. Saji, T.; Fukai, T.; Aoyagui, S. Polarography of tris(4,7-diphenyl-1,10-phenanthroline)-iron(II) complex. *J. Electroanal. Chem.* **1975**, *66*, 81–84. [CrossRef]
41. Simpson, T.C.; Durand, R.R., Jr. Ligand participation in the reduction of CO_2 catalyzed by complexes of 1,10 *o*-phenanthroline. *Electrochim. Acta* **1988**, *33*, 581–583. [CrossRef]
42. Azcarate, I.; Costentin, C.; Robert, M.; Savéant, J.M. Through-space charge interaction substituent effects in molecular catalysis leading to the design of the most efficient catalyst of CO_2-to-CO electrochemical conversion. *J. Am. Chem. Soc.* **2016**, *138*, 16639–16644. [CrossRef]
43. Lehn, J.M.; Ziessel, R. Photochemical generation of carbon monoxide and hydrogen by reduction of carbon dioxide and water under visible light irradiation. *PNAS* **1982**, *79*, 701–704. [CrossRef] [PubMed]
44. Allen, G.H.; White, R.P.; Rillema, D.P.; Meyer, T.J. Synthetic control of excited-state properties. tris-chelate complexes containing the ligands 2,2′-bipyrazine, 2,2′-bipyridine, and 2,2′-bipyrimidine. *J. Am. Chem. Soc.* **1984**, *106*, 2613–2620. [CrossRef]
45. Tamaki, Y.; Morimoto, T.; Koike, K.; Ishitani, O. Photocatalytic CO_2 reduction with high turnover frequency and selectivity of formic acid formation using Ru(II) multinuclear complexes. *PNAS* **2012**, *109*, 15673–15678. [CrossRef]
46. Wang, W.; Zhang, J.X.; Wang, H.; Chen, L.J.; Bian, Z.Y. Photocatalytic and electrocatalytic reduction of CO_2 to methanol by the homogeneous pyridine-based systems. *Appl. Catal. A Gen.* **2016**, *520*, 1–6. [CrossRef]

47. Wang, C.-J.; Cao, S.; Qin, B.; Zhang, C.; Li, T.-T.; Fu, W.-F. Photoreduction of iron(III) to iron(0) nanoparticles for simultaneous hydrogen evolution in aqueous solution. *ChemSusChem* **2014**, *7*, 1924–1933. [CrossRef] [PubMed]
48. Wang, C.-J.; Cao, S.; Fu, W.-F. A stable dual-functional system of visible-light-driven Ni(II) reduction to a nickel nanoparticle catalyst and robust in situ hydrogen production. *Chem. Commun.* **2013**, *49*, 11251–11253. [CrossRef] [PubMed]
49. Tamaki, Y.; Koike, K.; Morimoto, T.; Ishitani, O. Substantial improvement in the efficiency and durability of a photocatalyst for carbon dioxide reduction using a benzoimidazole derivative as an electron donor. *J. Catal.* **2013**, *304*, 22–28. [CrossRef]
50. Dong, J.; Wang, M.; Li, X.; Chen, L.; He, Y.; Sun, L. Simple nickel-based catalyst systems combined with graphitic carbon nitride for stable photocatalytic hydrogen production in water. *ChemSusChem* **2012**, *5*, 2133–2138. [CrossRef]
51. Behar, D.; Dhanasekaran, T.; Neta, P.; Hosten, C.M.; Ejeh, D.; Hambright, P.; Fujita, E. Cobalt porphyrin catalyzed reduction of CO_2. Radiation chemical, photochemical, and electrochemical studies. *J. Phys. Chem. A* **1998**, *102*, 2870–2877. [CrossRef]
52. Schneider, T.W.; Ertem, M.Z.; Muckerman, J.T.; Boza, A.M.A. Mechanism of photocatalytic reduction of CO_2 by Re(bpy)$(CO)_3$Cl from differences in carbon isotope discrimination. *ACS Catal.* **2016**, *6*, 5473–5481. [CrossRef]
53. Liu, G.G.; Meng, X.G.; Zhang, H.B.; Zhao, G.X.; Pang, H.; Wang, T.; Li, P.; Kako, T.; Ye, J.H. Elemental boron for efficient carbon dioxide reduction under light irradiation. *Angew. Chem. Int. Ed.* **2017**, *56*, 5570–5574. [CrossRef] [PubMed]

Sample Availability: Samples of the compounds are available from the authors.